



OPEN

Theoretical investigation of hybrid nanomaterials transient flow through variable feature of Darcy–Forchheimer space with exponential heat source and slip condition

Ikram Ullah¹, Yahya Alajlani², Amjad Ali Pasha³, Mohammad Adil^{4,5} & Wajaree Weera⁶✉

Nanomaterials have achieved remarkable importance in cooling small electronic gadgets like akin and microchips devices. The role of nanoparticles is essential in various aspects, especially in biomedical engineering. Thus hybrid nanomaterials is introduced to strengthen the heat exchangers' performance. In view of the above practical and existing applications of nanomaterials. Our aim is to examine the consequences of Darcy–Forchheimer's radiative and Hall current flow of nanomaterials over a rotating porous disk with variable characteristics. Stretching disk accounting for the slip condition. Nanoparticles ZnO and CoF₂O₄ are dispersed in based fluid water. The present model is utilized for thermo-physical attributes of hybrid nanomaterials with the impact of shape factor. Transformations convert the modeled PDEs into ODEs. The obtained highly non-linear system is tackled numerically by the NDSolve technique through the software Mathematica. The outcomes of significant variables against different profiles are executed and elaborated in detail. Obtained results show that both nano and hybrid nanofluid radial velocity have reverse behavior against variable porosity and permeability parameters, whereas it decays for larger Forchheimer numbers. Further, it is worthy to point out that, hybrid nanophase has a higher impact on distinct profiles when compared with nano and common liquid phases.

List of symbols

u, v, w	Components of velocity
Ω	Angular velocity
Re_r	Local Reynolds number
σ^*	Coefficient of mean absorption.
k^*	Steffman Biltzmann constant
L_1	Slip factor
Pr	Prandtl number
ρ	Density of fluid
CoF_2O_4	Cobalt ferrite
$g(\eta)$	Dimensionless axial velocity
m	Hall current parameter
Q_E	Heat source variable

¹Department of Sciences and Humanities, National University of Computer and Emerging Sciences, Peshawar 25000, KP, Pakistan. ²Department of Physics, Faculty of Science, Jazan University, Jazan, Saudi Arabia. ³Aerospace Engineering Department, King Abdulaziz University, Jeddah 21589, Saudi Arabia. ⁴Mechanical Engineering Program, Physical Science and Engineering Division, King Abdullah University of Science and Technology, Thuwal 23955-6900, Saudi Arabia. ⁵KAUST Clean Combustion Research Center, King Abdullah University of Science and Technology, Thuwal 23955-6900, Saudi Arabia. ⁶Department of Mathematics, Faculty of Science, Khon Kaen University, Khon Kaen 40002, Thailand. ✉email: wajawe@kku.ac.th

q_r	Radiative heat flux
p_e	Electron pressure
m_1	Exponential index
ν	Kinematic viscosity
nf	Nano fluid
EHS	Exponential heat source
ω	Rotational variable
B_o	Magnetic field strength
hmf	Hybrid nanofluid
f	Fluid
μ_e	Electron magnetic permeability
T_o	Origin temperature
s	Shape factor of nanoparticles
C_{fr}	Skin friction in radial direction
r, ϕ, z	Cylindrical coordinates
σ	Fluid electrical conductivity
T_s	Surface temperature
k	Thermal conductivity
Ec	Eckert number
c_b	Drag factor
Nu_r	Nusselt number
τ_e	Electron collision time
$\theta(\eta)$	Dimensionless temperature
F_r	Local inertia parameter
$f'(\eta)$	Dimensionless radial velocity
ZnO	Zinc oxide
k^{**}	Permeability of porous space
∞	Ambient condition
d_1	Variable permeability
c_p	Specific heat
c	Stretching rate
b	Dimensional positive constant
ε_∞	Constant porosity
d_2	Variable porosity
k_∞	Constant permeability
ω_e	Cyclotron frequency of electron
T	Fluid temperature
Q_0	Heat generation/absorption
γ_s	Slip parameter
C_{gr}	Skin friction in tangential direction

An advancement in heat transportation phenomenon through liquids is the main issue in various industrial and technologically system. Because such liquids are widely utilized in many industries. These liquids are addressed to be functioning liquid in machinery system, electronic devices and have several significant applications like thermal energy accumulation and elimination from one section of machine to another. However the low thermal features of these fluids is the key problem facing in the transportation of heat phenomenon. In order to resolve this complexity, various scientist added some solid particles having size less than 100 nm in the traditional liquids which shows high thermal characteristics when compared with base liquid. This special material is term as nano-liquids. Different researchers utilized different nanoparticles in the common liquid to explore the thermal features of liquid with various aspects. Hybrid nano materials are basically the composition of more than one nano-particles in base liquid. This nano-liquid gives highly efficient energy compared to that of common nano-liquid. In this regard Ramesh et al.¹ developed the mathematical relations describing the hybrid nanomaterials flow. Theoretical analysis of both nano and hybrid nano fluid was scrutinized by kumar et al.². Few novel attempts readings hybrid nanomaterials are³⁻³⁰.

Hall phenomena have gained remarkable attention owing to their uses in astrophysical, geophysical and engineering problems like Hall aspect in sensors and Hall accelerators etc. In the existence of strong magnetic field or in rarefied medium, the features of Hall current cannot be ignored. The trend of current for the use of MHD is towards strong field of magnet (In this case the effect of electromagnetic for is remarkable) and trend to less density of field like in nuclear fusion space light. In view of above constrain, the Hall current becomes significant³⁰. The important use of Hall current in medical science i.e. in MRI, ECG etc. Katagiri³¹ analyzed the impact of Hall current in MHD flow over a semi-infinite plate. Here applications of Hall current is analyzed. The results of the analysis revealed that Hall parameter has decreasing effect on blood flow, but opposite effect is noted with the increasing Hartmann number³². Mahdy et al.³³. discussed the features of Hall current on micro-temperature in a semi-conductor space. It has been examined from the study that variation in Hall current have a significant impact on velocity. Sabu et al.³⁴ statistically explored the Hall current phenomenon on ferro-liquid flow through inclined channel. Hall current has a decay effect on skin friction. The 3D Casson magnetized nanomaterials flow with ion slip and Hall features is examined by Ibrahim and Anbessa³⁵. Currently Ullah et al.³⁶ discussed the ion slip and Lorentz force effects on peristaltic channel.

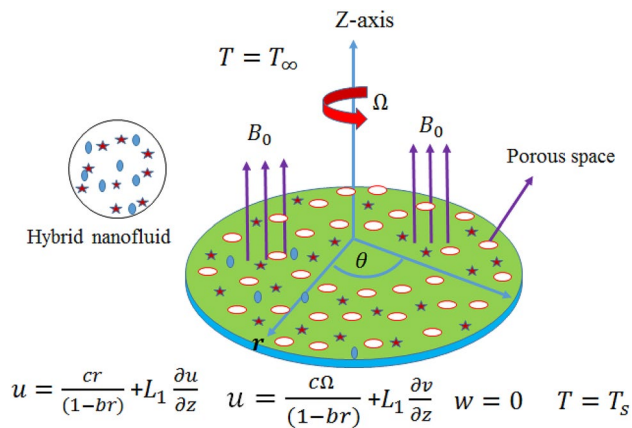


Figure 1. Flow physical configuration.

Heat transfer improvement in hybrid nanomaterials flow through porous space have numerous utilization in the various areas like petroleum, environmental, civil and biomedical engineering and agricultural etc. Production of oil and gas from reservoirs, water pollution through toxic liquids, irrigation and drainage, infrastructure construction, bio sensors and petrochemicals are the some significant applications. Flow through porous systems has been modeled by utilizing Darcy's law extensively. The flow converted to non-Darcian, when the Reynolds number exceeds unity, because the inertial aspect cause extra hydrodynamic head loss. In 1901 a Dutch researcher Forchheimer, dispense his ideas and expressions more extensively. Additionally he admitted the squared velocity term in the momentum expression to compute the inertial forces³⁷. Muskat³⁸ named this term as Forchheimer term. Few development in this area can be viewed^{39–44}. Heat transportation analysis in variable porous space is discussed by Vafai⁴⁵. After that Vafai et al.⁴⁶ performed the experimental inspection of flow via porous space subjected variable features. Ress and Pop⁴⁷ explored the variable permeability effects on a vertical free surface. Hayat et al.⁴⁸ examined the transient nanomaterial flow through porous regime with variable characteristics. Very recently, Ullah et al.⁴⁹ the nanomaterials flow through Darcy–Forchheimer (DF) space with varying permeability.

This work presents the Hall current and Lorentz force on flow of hybrid nanofluid ($CoF_2O_4 - ZnO/water$) over slippery and rotating porous disk with variable permeability. The key motivations of executing presents study are summarized as:

- Explore the Lorentz force and Hall current applications for hybrid nanoliquid flow subject to a porous disk.
- Novel features of CoF_2O_4 and ZnO conveying water hybrid nanomaterials.
- Darcy–Forchheimer law with variable porosity and permeability features is considered as a novelty.
- To investigate the thermal performance of hybrid nanomaterial with EHS, dissipation and radiation impacts.
- To discuss the rate of heat transportation with different shape of nanoparticles.
- Slippery constrains are imposed to examine the fluid flow.
- The numerical simulations are executed by utilizing the built in shooting techniques.
- The inspection of liquid with addition of two different nanoparticles is useful in machinery system, electronic devices, medical equipment's and treatment of diseases.

Problem formulation

Consider the magnetized hybrid nanofluid flow through a spinning and slippery porous disk. Fluid flow via Darcy–Forchheimer porous space is assumed with variable features. The porous disk rotates with an angular velocity (Ω) and stretch at $z = 0$ (see Fig. 1), which causes the hybrid nanomaterials motion. The surface of porous disk is sustain at temperature T_s and ambient temperature is T_∞ . The hybrid nanomaterials is the suspension of two kinds of nanomaterials CoF_2O_4 and ZnO in water. Hall current is the result of higher magnetic field applied normally to the disk. Impact of radiation, EHS and dissipation are additionally considered to examine the variation in temperature gradient comprehensively. Keeping in mind the aforementioned assumptions, the Hall current and Ohm's law relations are:

$$B(t) = \frac{B_0}{(1-bt)^{\frac{1}{2}}}, u = \frac{cr}{(1-bt)} + L_1 \frac{\partial u}{\partial z}, v = \frac{r\Omega}{(1-bt)} + L_1 \frac{\partial v}{\partial z}, T_s = T_o - T_{ref} \frac{r^2 \Omega}{v_f (1-bt)^{\frac{3}{2}}}. \quad (1)$$

$$\frac{\omega_e \tau_e}{B_0} (J \times B) + J = \sigma \left[\frac{1}{en_e} \nabla p_e + \mu_e (V \times B) \right], \quad (2)$$

The electric field is considered to be zero, taking the weakly ionized gas with negligible slip conditions and thermoelectric pressure. So the Hall current in component form are:

$$J_r = \frac{\mu_e \sigma B_o}{(1 + m^2)}(mv - u), \tag{3}$$

$$J_\varphi = \frac{\mu_e \sigma B_o}{(1 + m^2)}(mv + v), \tag{4}$$

In above equations, B manifests the magnetic induction, J the vector for current density, (T_s, T_{ref}, T_o) the surface, constant reference, origin temperatures respectively, (b, c) denote stretching rates, B_o magnetic field strength, ω_e cyclotron frequency of electron, τ_e electron collision time, p_e the electronic pressure, μ_e the magnetic permeability, n_e the number of density of electron, σ electrical conductivity of fluid and m the Hall current parameter. Hall current and the electrical conductivity and hall current expressions are $\sigma = \frac{e^2 n_e \tau_e}{m_e}$ and $m = \omega_e \tau_e$. The flow expressions for current analysis are^{30,49}:

$$\frac{\partial w}{\partial z} + \frac{1}{r} \frac{\partial}{\partial r}(ur) = 0, \tag{5}$$

$$\frac{\partial u}{\partial t} - \frac{v^2}{r} + w \frac{\partial u}{\partial z} + u \frac{\partial u}{\partial r} = v_{hnf} \left(\frac{\partial^2 u}{\partial z^2} \right) - \frac{\sigma_{hnf} B_o^2}{\rho_{hnf} (1 + m^2) (1 - bt)^{\frac{1}{2}}} (u - mv) - \frac{\varepsilon(z) v_{hnf}}{k^{**}(z)} u - \frac{\varepsilon^2(z) C_b}{\sqrt{k^{**}(z)}} u \sqrt{u^2 + v^2}, \tag{6}$$

$$\frac{\partial v}{\partial t} + u \frac{\partial v}{\partial r} + \frac{uv}{r} + w \frac{\partial v}{\partial z} = v_{hnf} \left(\frac{\partial^2 v}{\partial z^2} \right) - \frac{\sigma_{hnf} B_o^2}{\rho_{hnf} (1 + m^2) (1 - bt)^{\frac{1}{2}}} (v + mu) - \frac{\varepsilon(z) v_{hnf}}{k^{**}(z)} v - \frac{\varepsilon^2(z) C_b}{\sqrt{k^{**}(z)}} v \sqrt{u^2 + v^2}, \tag{7}$$

$$\begin{aligned} \frac{\partial T}{\partial t} + u \frac{\partial T}{\partial r} + w \frac{\partial T}{\partial z} &= \frac{k_{hnf}}{(\rho c_p)_{hnf}} \left(\frac{\partial^2 T}{\partial z^2} \right) - \frac{1}{(\rho c_p)_{hnf}} \frac{\partial q_r}{\partial z} \\ &+ Q_o (T_o - T_\infty) e^{\left(-m_1 \left(\sqrt{\frac{\Omega}{v_f(1-bt)}} z \right) \right)} + \frac{\mu_{hnf}}{(\rho c_p)_{hnf}} \left[\left(\frac{\partial u}{\partial z} \right)^2 - \left(\frac{\partial v}{\partial z} \right)^2 \right], \end{aligned} \tag{8}$$

$$k^{**}(z) = k_\infty \left(1 + d_1 e^{-\frac{z}{\gamma}} \right), \tag{9}$$

$$\varepsilon(z) = \varepsilon_\infty \left(1 + d_2^* e^{-\frac{z}{\gamma}} \right). \tag{10}$$

The radiative heat flux, which is given by:

$$q_r = -\frac{4\sigma^*}{3k^*} \frac{\partial T^4}{\partial z} = -\frac{16T_\infty^3 \sigma^*}{3k^*} \left(\frac{\partial T}{\partial z} \right), \tag{11}$$

From Eqs. (11) and (8), one has

$$\begin{aligned} \frac{\partial T}{\partial t} + u \frac{\partial T}{\partial r} + w \frac{\partial T}{\partial z} &= \frac{k_{hnf}}{(\rho c_p)_{hnf}} \left(\frac{\partial^2 T}{\partial z^2} \right) + \frac{\mu_{hnf}}{(\rho c_p)_{hnf}} \left[\left(\frac{\partial u}{\partial z} \right)^2 - \left(\frac{\partial v}{\partial z} \right)^2 \right] \\ &+ \frac{16\sigma^* T_\infty^3}{3k^* (\rho c_p)_{hnf}} \left(\frac{\partial^2 T}{\partial z^2} \right) + Q_o (T_o - T_\infty) e^{\left(-m_1 \left(z \sqrt{\frac{\Omega}{v_f(1-bt)}} \right) \right)}. \end{aligned} \tag{12}$$

where $F = c_b/r(k^{**})^{\frac{1}{2}}$ represents non-uniform inertia factor, ε_∞ stands for constant porosity, k_∞ stands for constant permeability, d_2 for variable porosity, T denotes fluid temperature, d_1 for the variable permeability, σ_{hnf} is hybrid nanofluid electric conducting, k_{hnf} denotes hybrid nanomaterials thermal conductivity, ρ_{hnf} is the density, L_1 denotes velocity slip factor, Q_o the heat generation/absorption parameter, c_b is drag factor, k^{**} is permeability of porous space, $(\rho c_p)_{hnf}$ is heat capacity of hybrid nanofluid, q_r is radiative heat flux, m_1 the exponential index, σ^* the coefficient of mean absorption, v_{hnf} denotes kinematics viscosity, $\gamma = \sqrt{\frac{v_f(1-bt)}{\Omega}}$ is the dimensional constant having dimension of length, and k^* manifest the constant of Stefan Boltzmann.

The specified conditions are:

$$\begin{aligned} (u, v, w, T) &= \left(L_1 \frac{\partial u}{\partial z} + \frac{cr}{(1-br)}, L_1 \frac{\partial v}{\partial z} + \frac{r\Omega}{(1-br)}, 0, T_s \right) \text{ at } z = 0 \\ u = 0, v = 0, T_\infty = T &\text{ as } z \rightarrow \infty, \end{aligned} \tag{13}$$

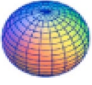




Shape	Sphere	Tetrahedron	Cylinder	column	Lamina
Geometry					
Shape factor	3.0	4.6	4.9	6.3598	16.1676

Table 1. Shape factor of nanoparticles⁵⁰.

	ρ (kg/m ³)	k (W/mk)	C_p (J/kgK)	σ (Ωm) ⁻¹
Pure water	997.1	0.613	4179	0.05
ZnO	5.606	19	544	0.01
CoF ₂ O ₄	4907	3.7	700	5.51×10^9

Table 2. The nanoparticles ZnO, CoF₂O₄ and water thermo-physical features^{51,52}.

Properties	Nanofluid	Hybrid nanofluid
Density	$\rho_{nf} = \rho_f \left((1 - \phi_1) + \phi_1 \left(\frac{\rho_z}{\rho_f} \right) \right)$	$\rho_{hnf} = \rho_f (1 - \phi_1) \left((1 - \phi_2) + \phi_1 \left(\frac{\rho_{ZnO}}{\rho_f} \right) \right) + \phi_2 \rho_{CoF_2O_4}$
Viscosity	$\mu_{nf} = \frac{\mu_f}{(1 - \phi_1)^{2.5}}$	$\mu_{hnf} = \frac{\mu_f}{(1 - \phi_1)^{2.5} (1 - \phi_2)^{2.5}}$
Heat capacity	$(\rho c_p)_{nf} = (\rho c_p)_f \left(1 - \phi_1 + \phi_1 \frac{(\rho c_p)_{ZnO}}{(\rho c_p)_f} \right)$	$(\rho c_p)_{nf} = \phi_2 (\rho c_p)_{CoF_2O_4} + (\rho c_p)_f (1 - \phi_2) \left((1 - \phi_1) + \phi_1 \frac{(\rho c_p)_{ZnO}}{(\rho c_p)_f} \right)$
Thermal conductivity	$\frac{k_{nf}}{k_f} = \frac{k_{ZnO} + (s-1)k_f - (s-1)\phi_1(k_f - k_{ZnO})}{k_{ZnO} + (s-1)k_f + \phi_1(k_f - k_{ZnO})}$	$\frac{k_{hnf}}{k_f} = \frac{k_{ZnO}(s-1)k_f - (s-1)(k_{bf} - k_{CoF_2O_4})\phi_2}{k_{ZnO} + (s-1)k_{bf} + \phi_2(k_{bf} - k_{CoF_2O_4})}$ where $\frac{k_{bf}}{k_f} = \frac{k_{CoF_2O_4} + (s-1)k_f - (s-1)(k_f - k_{CoF_2O_4})\phi_1}{k_{CoF_2O_4} + (s-1)k_f + \phi_1(k_f - k_{CoF_2O_4})}$
Electrical conductivity	$\frac{\sigma_{nf}}{\sigma_f} = 1 + \frac{3(\sigma - 1)\phi_1}{(\sigma + 2) - (\sigma - 1)\phi_1}$ where $\sigma = \frac{\sigma_{ZnO}}{\sigma_f}$	$\frac{\sigma_{hnf}}{\sigma_f} = \frac{\sigma_{CoF_2O_4} + 2\sigma_{bf} - 2\phi_2(\sigma_{bf} - \sigma_{CoF_2O_4})}{\sigma_{CoF_2O_4} + 2\sigma_{bf} + \phi_2(\sigma_{bf} - \sigma_{CoF_2O_4})}$ where $\frac{\sigma_{bf}}{\sigma_f} = \frac{\sigma_{ZnO} + 2\sigma_f - 2\phi_1(\sigma_f - \sigma_{ZnO})}{\sigma_{ZnO} + 2\sigma_f + \phi_1(\sigma_f - \sigma_{ZnO})}$

Table 3. Thermo-physical relations for nano and hybrid nanofluids^{29,41}.

Nano and Hybrid nanomaterials properties. The shape factor of nanoparticles is displayed in Table 1. The physical characteristics and relations of nano and hybrid nanomaterials are summarized in Tables 2 and 3 respectively.

Transformations. The following transformations are introduced for current study³⁰:

$$\eta = \sqrt{\frac{\Omega}{v_f(1 - bt)}}z, v = \frac{r\Omega}{(1 - bt)}g(\eta)$$

$$u = \frac{r\Omega}{(1 - bt)}f'(\eta), T = T_o - T_{ref} \left(\frac{r^2\Omega}{v_f(1 - bt)^{\frac{3}{2}}} \right) \theta(\eta) \tag{14}$$

$$w = -2 \left(\frac{v_f\Omega}{1 - bt} \right)^{\frac{1}{2}} f(\eta),$$

Employing the Eq. (11) in Eqs. (5–12) becomes

	Yin et al. ⁵³	Turkyilmazoglu ⁵⁴	Present outcomes
$f'(0)$	0.51022941	0.51023262	0.51024311
$-g'(0)$	0.61591990	0.61592201	0.61591032
$-\theta'(0)$	0.93387285	0.93387794	0.93376327

Table 4. Comparative studies of $-\theta'(0)$, $-g'(0)$ and $f'(0)$ with^{53,54}.

$$\begin{aligned} & \frac{A_1}{A_2} f''' + (g^2 + 2ff'' - f'^2) - S\left(\frac{\eta}{2} f'' + f'\right) - \frac{A_3}{A_2(1+m^2)} M(f' - mg) \\ & - \frac{A_1}{A_2} \frac{1}{\text{Re}_r \alpha} \left(\frac{1+d_2 e^{-\eta}}{1+d_1 e^{-\eta}}\right) f' - F_r \frac{(1+d_2 e^{-\eta})^2}{\sqrt{1+d_1 e^{-\eta}}} (f'^2 + g^2) = 0, \end{aligned} \tag{15}$$

$$\begin{aligned} & \frac{A_1}{A_2} g'' - 2(fg' - f'g) - S\left(\frac{\eta}{2} g' + g\right) - \frac{A_3}{A_2(1+m^2)} M(g - mf') \\ & - \frac{A_1}{A_2} \frac{1}{\text{Re}_r \alpha} \left(\frac{1+d_2 e^{-\eta}}{1+d_1 e^{-\eta}}\right) g - F_r \frac{(1+d_2 e^{-\eta})^2}{\sqrt{1+d_1 e^{-\eta}}} (f'^2 + g^2) = 0, \end{aligned} \tag{16}$$

$$\begin{aligned} & A_4 \left(A_5 + \frac{4}{3} Rd\right) \theta'' - \text{Pr} S\left(\frac{\eta}{2} \theta' + \frac{3}{2} \theta\right) + 2 \text{Pr}(f\theta' - f'\theta) \\ & + \text{Pr} Q_E e^{(-m_1 \eta)} - \frac{A_4}{A_1} \text{Pr} Ec(f'^2 + g'^2) = 0. \end{aligned} \tag{17}$$

With

$$\begin{aligned} & f = 0, \quad f' = \omega + \gamma_s f''(0), \quad g = 1 + \gamma_s g'(0), \quad \theta(0) = 1, \quad \text{at } \eta = 0, \\ & f' = 0, \quad g = 0, \quad \theta = 0, \quad \text{as } \eta \rightarrow 0, \end{aligned} \tag{18}$$

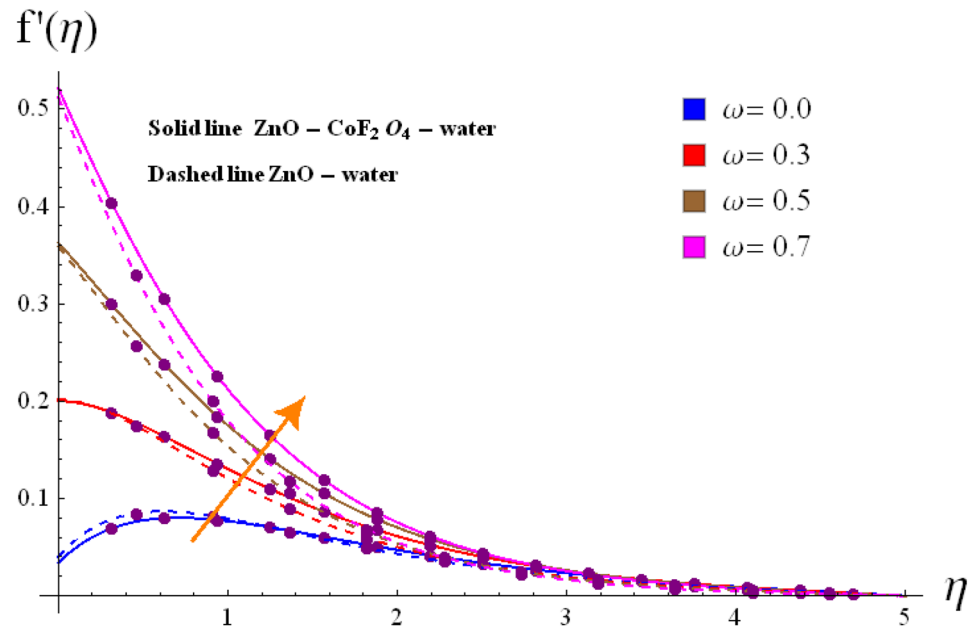
where, F_r stands for local inertia variable, α for porosity parameter, ω is rotational variable, S measure unsteadiness, M is magnetics variable, m denotes Hall current variable, γ_s is slip parameter, Rd denotes radiation parameter, Pr is Prandtl number $\text{Pr} = 6.5$ for water, F_r denotes Forchheimer number and Ec stands for Eckert number. The dimensionless variables and A_1, A_2, A_3, A_4 and A_5 are expressed as:

$$\begin{aligned} Q_E &= \frac{Q_0}{(\rho_f c_p)_{hmf} \Omega}, \quad \gamma_s = L_1 \sqrt{\frac{\Omega}{\nu_f(1-bt)}}, \quad F_r = \frac{\varepsilon_\infty r c_b}{\sqrt{k_\infty}}, \quad \alpha = \frac{k_\infty}{r^2 \varepsilon_\infty}, \quad S = \frac{b}{\Omega}, \quad \omega = \frac{\Omega}{c}, \quad m = \omega_e \tau_e, \\ M &= \frac{\sigma_1 B_o^2}{\rho_f \Omega}, \quad \text{Pr} = \frac{\mu_f (\rho C_p)_f}{\rho_f k_f}, \quad Rd = \frac{4\sigma^* (T_\infty^3)}{k^* k_f}, \quad Ec = \frac{r^2 \Omega^2}{(T_s - T_o)(1-bt)^2}, \quad A_1 = \frac{\mu_{hmf}}{\mu_f}, \\ A_2 &= \frac{\rho_{hmf}}{\rho_f}, \quad A_3 = \frac{\sigma_{hmf}}{\sigma_f}, \quad A_4 = \frac{(\rho C_p)_f}{(\rho C_p)_{hmf}}, \quad A_5 = \frac{k_{hmf}}{k_f} \end{aligned} \tag{19}$$

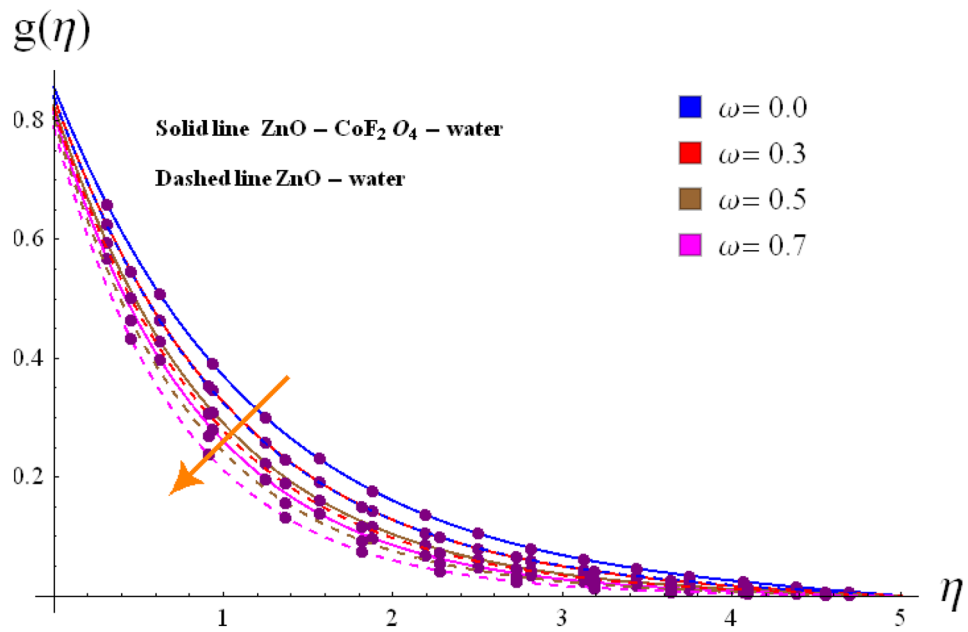
Engineering quantities. The surface transport aspects focusing the current hybrid nanomaterials flow is inspected locally with help of skin frictions (C_{fr}, C_{gr}) and Nusselt number (Nu_r) as follows:

$$\begin{aligned} C_{fr} &= \frac{2\mu_{hmf} \left(\frac{\partial u}{\partial z}\right)_{z=0}}{\rho_{hmf} \left(\frac{r\Omega}{1-bt}\right)^2}, \\ C_{gr} &= \frac{2\mu_{hmf} \left(\frac{\partial v}{\partial z}\right)_{z=0}}{\rho_{hmf} \left(\frac{r\Omega}{1-bt}\right)^2}, \\ Nu_r &= \frac{r q_w}{k_{hmf} (T - T_\infty)} + (q_r)_{z=0}, \end{aligned} \tag{20}$$

where q_w designates the heat flux. After simplifications, the reduced quantities are:



(a)

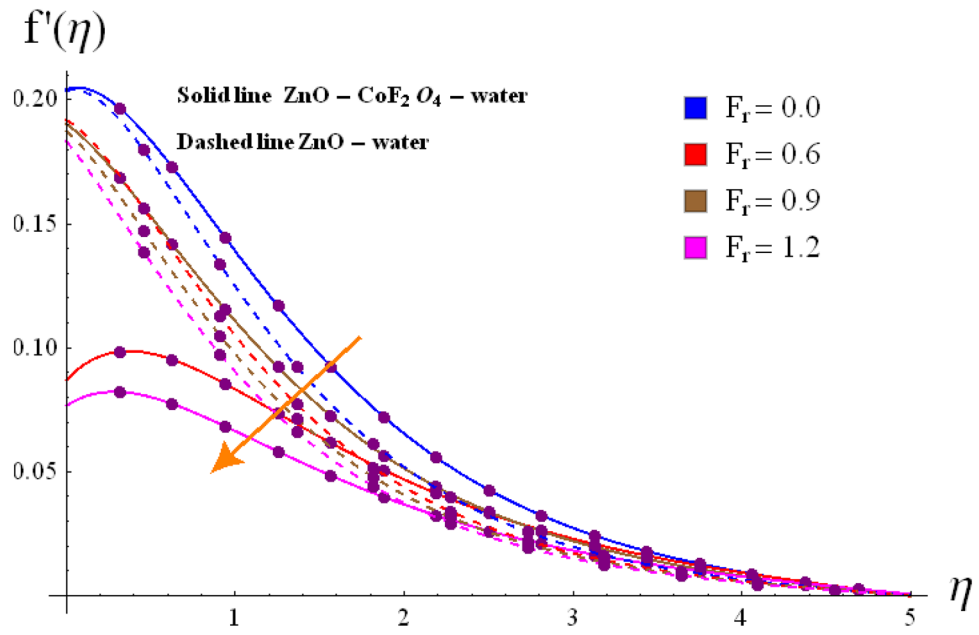


(b)

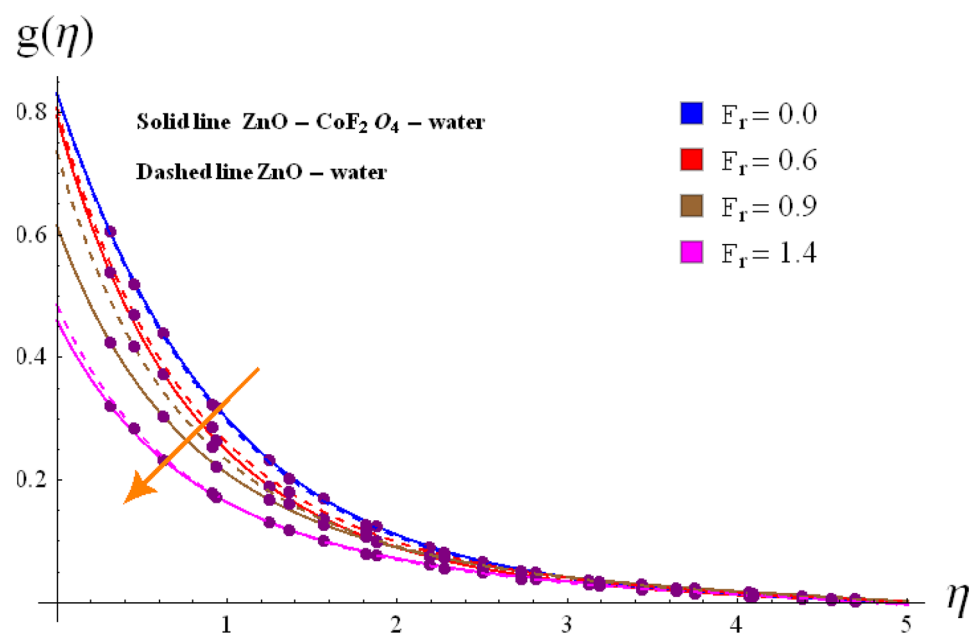
Figure 2. (a) Variation of $f'(\eta)$ via ω . (b) Variation of $g(\eta)$ via ω .

$$\begin{aligned} \text{Re}^{\frac{1}{2}} C_f &= \frac{f''(0)}{(1 - \phi_{Ni})^{2.5} (1 - \phi_{ZnO})^{2.5}}, \\ \text{Re}^{\frac{1}{2}} C_g &= \frac{g'(0)}{(1 - \phi_{Ni})^{2.5} (1 - \phi_{ZnO})^{2.5}}, \\ \text{Re}^{-\frac{1}{2}} Nu_r &= -\left(\frac{k_{hnf}}{k_f}\right) \left(1 - \frac{4}{3} Rd\right) \theta'(0). \end{aligned} \tag{21}$$

where $\text{Re} = \frac{r^2 \Omega}{\nu_f (1 - bt)}$ present the Reynold number.



(a)



(b)

Figure 3. (a) Variation of $f'(\eta)$ via F_r . (b) Variation of $g(\eta)$ via F_r .

Methodology and validation of outcomes

The converted system in Eqs. (15–19) are non-linear and coupled, therefore close form solution is indeed difficult⁹. To side up this issue, the transform ODEs are treated numerically via NDSolve technique, adopting the software Mathematica. Basically NDSolve is a built-in shooting technique, which can be process for small step sizes leads to less error. Present fallouts with published outcomes are compared to validate the current problem (see Table 4). It is identified that an excellent match between present outcomes and Yin et al.⁵³ and Turkyilmazoglu⁵⁴ is obtained.

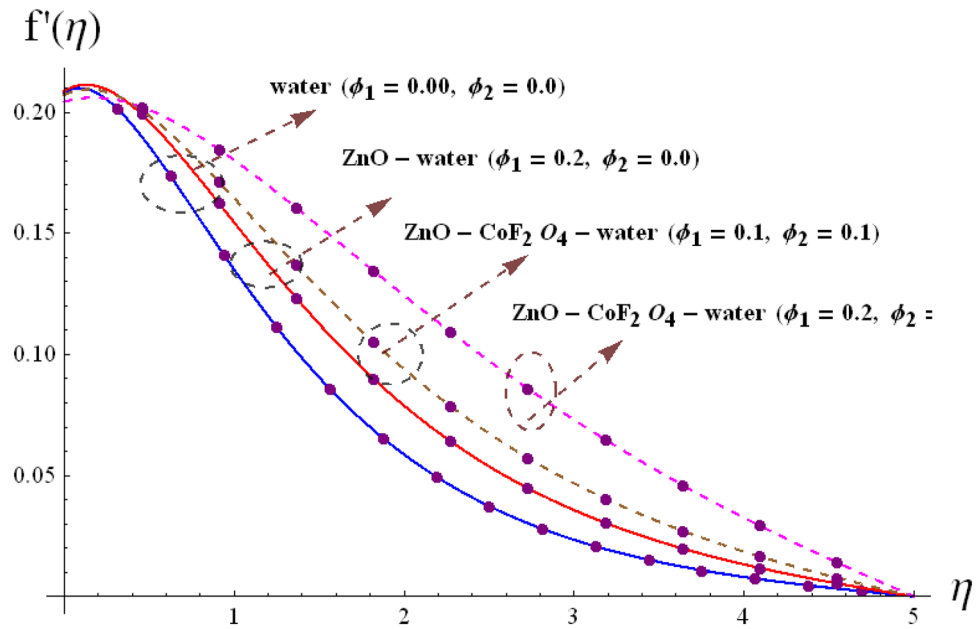


Figure 4. Variation of $f'(\eta)$ via ϕ_1/ϕ_2 .

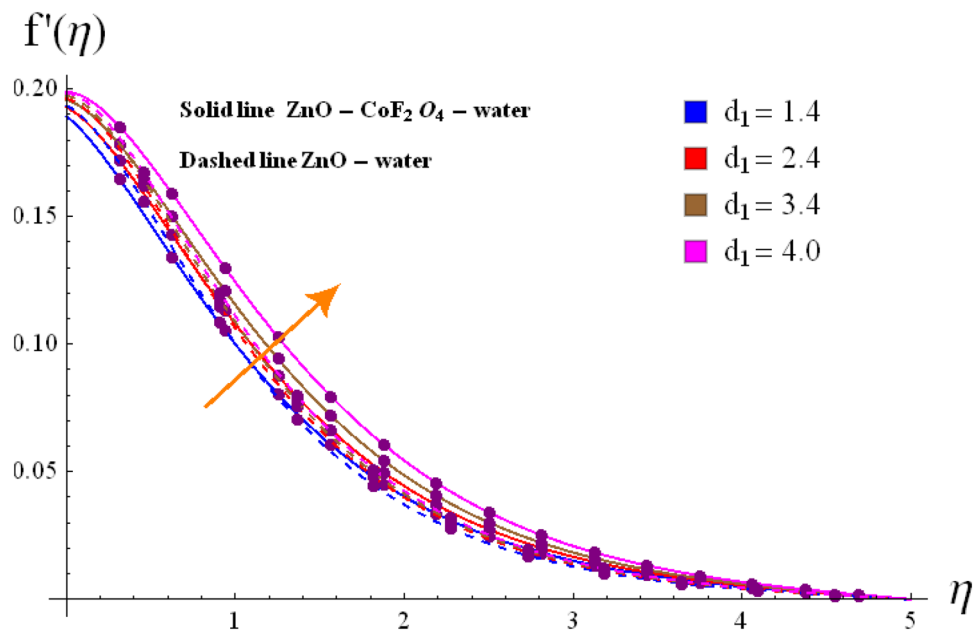


Figure 5. Variation of $f'(\eta)$ via d_1 .

Physical discussion of outcomes

Base on the previous numerical executions, many illustrative outcomes are designed in this section as depicted in Figs. 2, 3, 4, 5, 6, 7 and 8 for $f'(\eta), g(\eta), \theta(\eta)$ and $C_{f,r}$ and Nu_r against various estimations of interesting variables. For whole study, the default values of physical parameters are $\omega = 0.2, \gamma_s = 0.2, M = 0.2, Fr = 0.1, \alpha = 0.2, d_1 = d_2 = 0.5, m = 0.2, Rd = 0.2, m_1 = 0.1, Q_E = 0.25, Ec = 0.2, \phi_1 = 0.01,$ and $\phi_2 = 0.01$. Some numerical values are assigning to each parameter, while other parameters are kept unchanged. Curves for hybrid and nano phases are denoted by solid and dashed lines respectively.

Velocity interpretation. The radial $f'(\eta)$ and tangential $g(\eta)$ velocities against ω, Fr, d_1, d_2 and ϕ_1/ϕ_2 are shown in Figs. 2, 3, 4, 5, 6, 7 and 8. Results for radial velocity $f'(\eta)$ versus ω is presented in Fig. 2a. Here rising the estimations of ω leads to enhance the nanofluid velocity. Rotation variable is the ratio of rotating rate to

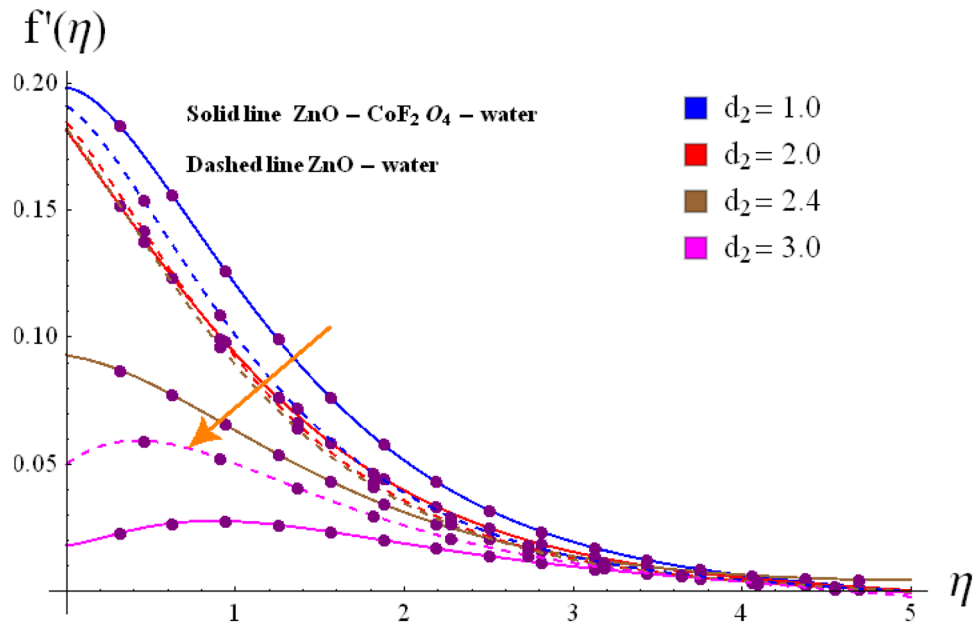


Figure 6. Variation of $f'(\eta)$ via d_2 .

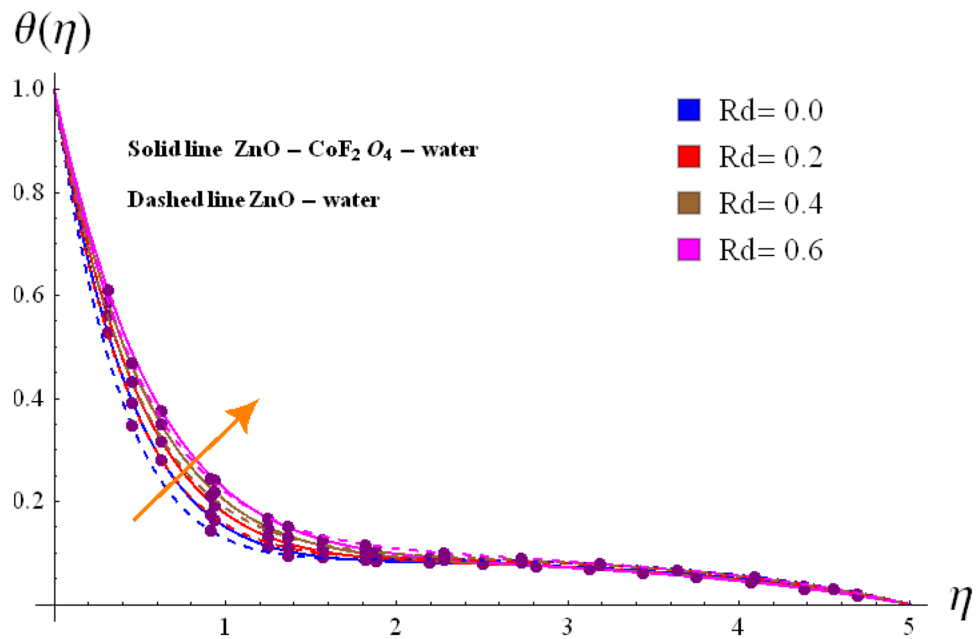


Figure 7. Variation of $\theta(\eta)$ via Rd .

stretching rate. Thus, larger estimations of ω implies higher rotation rate when compared with rate of stretching. In fact an increment in ω means enhancing the centrifugal force which consequently deploy pressure on nano-materials to boosts up the motion of liquid particles in the radiation direction, where the decaying behavior for tangential velocity $g(\eta)$ is seen in Fig. 2b. Fig. 3a, b illustrates the impact of Fr on $f'(\eta)$ and $g(\eta)$. It is noted that higher Fr corresponds decline $f'(\eta)$ and $g(\eta)$ in both nano and hybrid phases. In fact higher Fr leads to higher inertial force which decays both velocities. Comparative analysis of hybrid ($\phi_1 \neq 0, \phi_2 \neq 0$) and base liquid ($\phi_1 = 0, \phi_2 = 0$) on radial velocity $f'(\eta)$ is illustrated in in Fig. 4. Clearly hybrid nanofluid ($\phi_1 \neq 0, \phi_2 = 0$) have more parts in rising $f'(\eta)$ than the nano and base liquids. Figure 5 is schemed graphically to explore the dynamical features of hybrid and nano phases against d_1 . Boosting trend is observed in this sketch with growing estimation of d_1 .

Contrarily to the aforementioned impact, radial velocity $f'(\eta)$ shows diminishing behavior against d_2 for both cases of nanofluids.

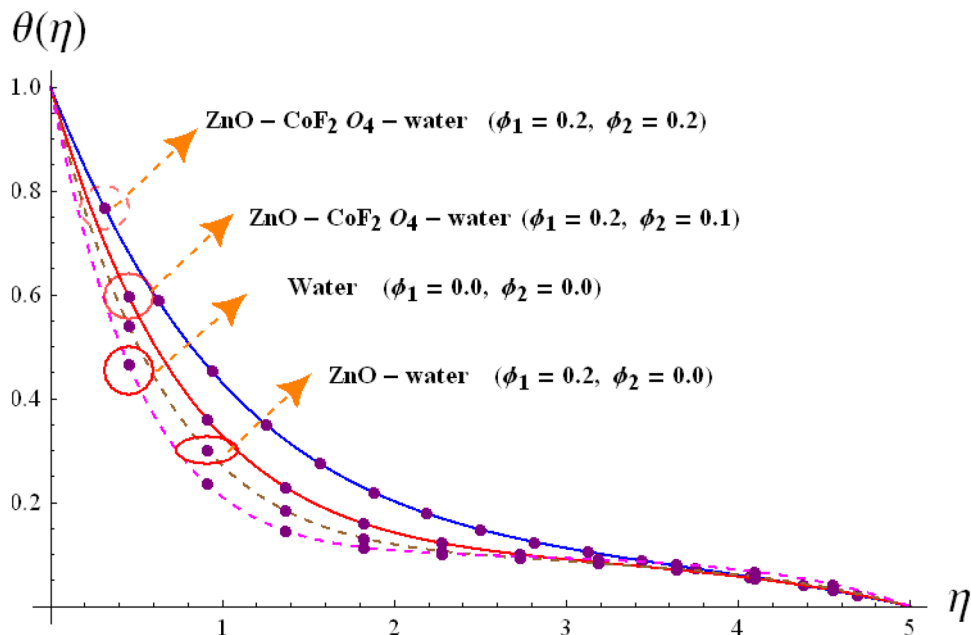


Figure 8. Variation of $\theta(\eta)$ via ϕ_1/ϕ_2 .

d_1	d_2	λ	F_r	ω	C_{f_r}		C_{g_r}	
					ZnO Water	ZnO - CoF ₂ O ₄ Water	ZnO Water	ZnO - CoF ₂ O ₄ Water
0.2	2.0	0.2	0.2	0.2	0.039018	0.055687	0.969356	1.138655
0.5					0.031256	0.046169	0.959022	1.123875
2.0					0.010282	0.011103	0.933633	1.075667
5.2	0.0	0.2	0.2	0.2	0.012797	0.007865	0.911227	1.055545
	0.2				0.005854	0.000062	0.916651	1.062424
	0.4				-0.00185	-0.00853	0.922603	1.066083
5.2	0.2	0.0	0.2	0.2	0.040515	0.035413	0.901291	1.044377
		0.3			-0.00957	-0.03073	0.916651	1.062424
		0.6			-0.000415	-0.05778	0.9314307	0.984552
5.2	0.2	0.2	0.0	0.2	0.0314713	0.028414	0.8650194	1.004653
			0.2		0.0058540	0.000062	0.9416488	1.117536
			0.4		-0.018760	0.111325	0.1119701	1.169940
5.2	0.2	0.2	0.2	0.0	0.2042584	0.226319	0.8181331	0.953427
				0.3	-0.101338	-0.12255	0.9609267	1.111851
				0.6	-0.451223	-0.52400	1.0782713	0.524002

Table 5. Skin frictions (C_{f_r} and C_{g_r}) numerical values versus various parameter.

Temperature interpretation. Figures 7 and 8 are designed to investigate the comparative analysis nano and hybrid nanomaterials on $\theta(\eta)$ against varying estimations of Rd and ϕ_1/ϕ_2 . The variation of Rd on $\theta(\eta)$ for hybrid and nano particles are structured in Fig. 7. It is shown that sharply increment in Rd boosts up thermal field due to more heat absorbed by hybrid nanofluid. Physically, higher Rd means more heat is provided to hybrid nanomaterials, that is why $\theta(\eta)$ enhances. The variation of $\theta(\eta)$ of hybrid nanofluid for rising estimations of ϕ_1/ϕ_2 is shaped in Fig. 8. Higher ϕ_1/ϕ_2 leads to boost the nano and hybrid nanofluid thermal field. This figure

Parameters			Nu_r				
Rd	d_1	QE	Shape factors effect on hybrid nanofluid				
			$s = 3$	$s = 4.6$	$s = 4.9$	$s = 6.3598$	$s = 16.1576$
0.2	5.0	0.2	2.669020	2.833824	2.86322	3.000252	3.72986
0.2			3.067484	3.292329	3.33232	3.518228	4.49681
0.4			3.418238	3.698038	3.74787	3.979717	5.20179
0.2	0.0	0.2	2.450075	1.274921	2.35187	3.414902	4.34628
	0.2		2.994185	1.186629	2.27522	3.427278	4.36405
	0.5		3.006047	1.110452	3.26226	3.441933	4.38519
0.2	5.0	0.0	0.456489	0.664149	0.77614	1.145939	4.84184
		0.1	3.067484	3.292329	3.33232	3.518264	4.49682
		0.2	2.834797	3.041641	3.07843	3.249546	4.15181

Table 6. Numerical data of (cNu_r) versus various parameters and shape factor.

also provide us comparative study for three different cases i.e. hybrid ($\phi_1 = 0, \phi_2 \neq 0$), nano ($\phi_1 \neq 0, \phi_2 = 0$) and base ($\phi_1 = 0, \phi_2 = 0$). Clearly hybrid nanoliquid dominates over the base and nano liquids.

Variation in physical quantities. The skin frictions of the hybrid and nano phases through distinct variables are disclosed in Table 5. It is detected that Cf_r and Cg_r have opposite trend for d_1 and d_2 . Furthermore, skin frictions are more in case of hybrid nanoliquid than the traditional nanoliquid. Table 6 designed the variations in Nusselt number with shape factor against several variables. Here it is seen that heat transfer rate is higher for lamina shaped nanoparticles.

Concluding remarks

Here significant features of variable porosity and permeability on hybrid nanofluid ($CoF_2O_4 - ZnO/water$) flow through Darcy–Forchheimer space with the impact of radiation, EHS and hall current is addressed. Main findings of current analysis are:

- Variable porosity and permeability have reverse behavior on $f'(\eta)$.
- Both radial and tangential velocities have opposite behavior for higher ω .
- Temperature is increasing for ϕ_1/ϕ_2 and Rd .
- Thermal field is higher for ($CoF_2O_4 - ZnO/water$) than (ZnO/H_2O) nanomaterials.
- Nusselt number is grows up more rapidly in case of lamina shape nanoparticles in comparison with other shape nano particles.
- Hybrid nanomaterials have dominant effect thought out the analysis than the ordinary one.
- Lamina shape of nanoparticle is more effective and improves the thermal field than other shapes.
- Present analysis can be extended by incorporating entropy analysis, ternary hybrid nanofluid, fractional modeling and different techniques as future work^{55–66}.

Received: 12 October 2021; Accepted: 3 August 2022

Published online: 05 September 2022

References

1. Buongiorno, J. Convective transport in nanofluids. *J. Heat Transf.* **128**, 240–250 (2006).
2. Dogonchi, A. S., Ismael, M. A., Chamkha, A. J. & Ganji, D. D. Numerical analysis of natural convection of Cu–water nanofluid filling triangular cavity with semicircular bottom wall. *J. Therm. Anal. Calorim.* **135**(6), 3485–3497 (2019).
3. Ullah, I., Ullah, R., Alqarni, M. S., Xia, W.-F. & Muhammad, T. Combined heat source and zero mass flux features on magnetized nanofluid flow by radial disk with the applications of Coriolis force and activation energy. *Int. Commun. Heat Mass Transf.* **126**, 105416 (2021).
4. Mahanthesh, B., Giresha, B. J., Animasaun, I. L., Muhammad, T. & Shashikumar, N. S. MHD flow of SWCNT and MWCNT nanoliquids past a rotating stretchable disk with thermal and exponential space dependent heat source. *Phys. Scr.* **94**(8), 085214 (2019).
5. Reza, J., Mebarek-Oudina, F. & Makinde, O. D. MHD slip flow of Cu–Kerosene nanofluid in a channel with stretching walls using 3-stage Lobatto IIIA formula. *Defect Diffus. Forum* **387**, 51–62 (2018).
6. Ullah, I., Hayat, T., Aziz, A. & Alsaedi, A. Significance of entropy generation and the coriolis force on the three-dimensional non-darcy flow of ethylene-glycol conveying carbon nanotubes (SWCNTs and MWCNTs). *J. Non Equilib. Thermodyn.* **47**(1), 61–75 (2022).
7. Mahanthesh, B., Giresha, B. J., Prasannakumara, B. C. & Sampath Kumar, P. B. Magneto-Thermo-Marangoni convective flow of Cu–H₂O nanoliquid past an infinite disk with particle shape and exponential space based heat source effects. *Results Phys.* **7**, 2990–2996 (2017).
8. Dogonchi, A. S., Nayak, M. K., Karimi, N., Chamkha, A. J. & Ganji, D. D. Numerical simulation of hydrothermal features of Cu–H₂O nanofluid natural convection within a porous annulus considering diverse configurations of heater. *J. Therm. Anal. Calorim.* **141**(5), 2109–2125 (2020).

9. Nayak, M. K., Mehmood, R., Mishra, S., Misra, A. & Muhammad, T. Thermal and velocity slip effects in mixed convection flow of magnetized ceramic nanofluids over a thin needle with variable physical properties. *Waves Random Complex Media* <https://doi.org/10.1080/17455030.2021.1983231> (2021).
10. Seyyedi, S. M., Dogonchi, A. S., Ganji, D. D. & Hashemi-Tilehnoee, M. Entropy generation in a nanofluid-filled semi-annulus cavity by considering the shape of nanoparticles. *J. Therm. Anal. Calorim.* **138**(2), 1607–1621 (2019).
11. Ali, B., Thumma, T., Habib, D. & Riaz, S. Finite element analysis on transient MHD 3D rotating flow of Maxwell and tangent hyperbolic nanofluid past a bidirectional stretching sheet with Cattaneo Christov heat flux model. *Therm. Sci. Eng. Prog.* **28**, 101089 (2022).
12. Ali, B. *et al.* Significance of Lorentz and Coriolis forces on dynamics of water based silver tiny particles via finite element simulation. *Ain Shams Eng. J.* **13**(2), 101572 (2022).
13. Sadeghi, M. S., Tayebi, T., Dogonchi, A. S., Nayak, M. K. & Waqas, M. Analysis of thermal behavior of magnetic buoyancy-driven flow in ferrofluid-filled wavy enclosure furnished with two circular cylinders. *Int. Commun. Heat Mass Transf.* **120**, 104951 (2021).
14. Nayak, M. K., Mabood, F., Dogonchi, A. S. & Khan, W. A. Electromagnetic flow of SWCNT/MWCNT suspensions with optimized entropy generation and cubic auto catalysis chemical reaction. *Int. Commun. Heat Mass Transf.* **120**, 104996 (2021).
15. Ullah, I., Shah, S. I., Zaman, G., Muhammad, T. & Hussain, Z. Passive control of magneto-nanomaterials transient flow subject to non-linear thermal radiation. *Therm. Sci.* **26**(2 Part B), 1405–1419 (2022).
16. Ramesh, G. K., Manjunatha, S., Roopa, G. S. & Chamkha, A. J. Hybrid (ND-Co3O4/EG) nanoliquid through a permeable cylinder under homogeneous-heterogeneous reactions and slip effects. *J. Therm. Anal. Calorim.* **146**(3), 1347–1357 (2021).
17. Kumar, K. G., Lokesh, H. J., Shehzad, S. A. & Ambreen, T. On analysis of Blasius and Rayleigh–Stokes hybrid nanofluid flow under aligned magnetic field. *J. Therm. Anal. Calorim.* **139**(3), 2119–2127 (2020).
18. Turkyilmazoglu, M. Single phase nanofluids in fluid mechanics and their hydrodynamic linear stability analysis. *Comput. Methods Programs Biomed.* **187**, 105171 (2020).
19. Khan, U., Zaib, A. & Mebarek-Oudina, F. Mixed convective magneto flow of SiO₂–MoS₂/C₂H₆O₂ hybrid nanoliquids through a vertical stretching/shrinking wedge: Stability analysis. *Arab. J. Sci. Eng.* **45**(11), 9061–9073 (2020).
20. Thriveni, K. & Mahanthes, B. Optimization and sensitivity analysis of heat transport of hybrid nanoliquid in an annulus with quadratic Boussinesq approximation and quadratic thermal radiation. *Eur. Phys. J. Plus* **135**(6), 1–22 (2020).
21. Gowda, R. J. P. *et al.* Thermophoretic particle deposition in time-dependent flow of hybrid nanofluid over rotating and vertically upward/downward moving disk. *Surf. Interfaces* **22**, 100864 (2021).
22. Mahanthes, B., Shehzad, S. A., Mackolil, J. & Shashikumar, N. S. Heat transfer optimization of hybrid nanomaterial using modified Buongiorno model: A sensitivity analysis. *Int. J. Heat Mass Transf.* **171**, 121081 (2021).
23. Jamshed, W. *et al.* Thermal efficiency enhancement of solar aircraft by utilizing unsteady hybrid nanofluid: A single-phase optimized entropy analysis. *Sustain. Energy Technol. Assess.* **52**, 101898 (2022).
24. Jamshed, W., Nasir, N. A. A. M., Brahmia, A., Nisar, K. S. & Eid, M. R. Entropy analysis of radiative [MgZn₂Zr–Cu/EO] Casson hybrid nanoliquid with variant thermal conductivity along a stretching surface: Implementing Keller box method. *Proc. Inst. Mech. Eng. Part C J. Mech. Eng. Sci.* <https://doi.org/10.1177/09544062211065696> (2022).
25. Bayones, F. S., Jamshed, W., Elhag, S. H. & Eid, M. R. Computational Galerkin finite element method for thermal hydrogen energy utilization of first grade viscoelastic hybrid nanofluid flowing inside PTSC in solar powered ship applications. *Energy Environ.* <https://doi.org/10.1177/0958305X221081463> (2022).
26. Bouslimi, J. *et al.* Dynamics of convective slippery constraints on hybrid radiative Sutterby nanofluid flow by Galerkin finite element simulation. *Nanotechnol. Rev.* **11**(1), 1219–1236 (2022).
27. Ouni, M., Ladhar, L. M., Omri, M., Jamshed, W. & Eid, M. R. Solar water-pump thermal analysis utilizing copper–gold/engine oil hybrid nanofluid flowing in parabolic trough solar collector: Thermal case study. *Case Stud. Therm. Eng.* **30**, 101756 (2022).
28. Shaw, S., Samantaray, S. S., Misra, A., Nayak, M. K. & Makinde, O. D. Hydromagnetic flow and thermal interpretations of cross hybrid nanofluid influenced by linear, nonlinear and quadratic thermal radiations for any Prandtl number. *Int. Commun. Heat Mass Transf.* **130**, 105816 (2022).
29. Ullah, I. Heat transfer enhancement in Marangoni convection and nonlinear radiative flow of gasoline oil conveying Boehmite alumina and aluminum alloy nanoparticles. *Int. Commun. Heat Mass Transf.* **132**, 105920 (2022).
30. Khan, M., Ali, W. & Ahmed, J. A hybrid approach to study the influence of Hall current in radiative nanofluid flow over a rotating disk. *Appl. Nanosci.* **10**, 5167–5177 (2020).
31. Katagiri, M. The effect of Hall currents on the magnetohydrodynamic boundary layer flow past a semi-infinite flat plate. *J. Phys. Soc. Jpn.* **27**(4), 1051–1059 (1969).
32. Das, S., Pal, T. K., Jana, R. N. & Giri, B. Ascendancy of electromagnetic force and Hall currents on blood flow carrying Cu–Au NPs in a non-uniform endoscopic annulus having wall slip. *Microvasc. Res.* **138**, 104191 (2021).
33. Mahdy, A. M. S., Lotfy, K., Ahmed, M. H., El-Bary, A. & Ismail, E. A. Electromagnetic Hall current effect and fractional heat order for microtemperature photo-excited semiconductor medium with laser pulses. *Results Phys.* **17**, 103161 (2020).
34. Sabu, A. S., Mathew, A., Neethu, T. S. & Anil George, K. Statistical analysis of MHD convective ferro-nanofluid flow through an inclined channel with hall current, heat source and solet effect. *Therm. Sci. Eng. Progress* **22**, 100816 (2021).
35. Ibrahim, W. & Anbessa, T. Three-dimensional MHD mixed convection flow of Casson nanofluid with hall and ion slip effects. *Math. Probl. Eng.* **2020**, 1–15 (2020).
36. Ullah, I., Shah, S. I., Alam, M. M., Sultana, N. & Pasha, A. A. Thermodynamic of Ion-slip and magnetized peristalsis channel flow of PTT fluid by considering Lorentz force and Joule heating. *Int. Commun. Heat Mass Transf.* **136**, 106163 (2022).
37. Forchheimer, P. H. *Wasserbewegung Durch Boden: Zeitschrift des Vereines Deutscher Ingenieure*, Vol. 45 1781–1788 (1901).
38. Muskat, M. *The Flow of Homogeneous Fluids Through Porous Media* (Edwards, 1946).
39. Ullah, M. Z., Serra-Capizzano, S. & Baleanu, D. A numerical simulation for Darcy–Forchheimer flow of nanofluid by a rotating disk with partial slip effects. *Front. Phys.* **7**, 219 (2020).
40. Ramesh, G. K. Three different hybrid nanometrial performances on rotating disk: A non-Darcy model. *Appl. Nanosci.* **9**(2), 179–187 (2019).
41. Ullah, I., Hayat, T. & Alsaedi, A. Optimization of entropy production in flow of hybrid nanomaterials through Darcy–Forchheimer porous space. *J. Therm. Anal. Calorim.* **147**, 5855–5864 (2021).
42. Bejawada, S. G. *et al.* 2D mixed convection non-Darcy model with radiation effect in a nanofluid over an inclined wavy surface. *Alex. Eng. J.* **61**(12), 9965–9976 (2022).
43. Rout, H. *et al.* Entropy optimization for Darcy–Forchheimer electro-magneto-hydrodynamic slip flow of ferro-nanofluid due to stretching/shrinking rotating disk. *Waves Random Complex Media* <https://doi.org/10.1080/17455030.2021.1927238> (2021).
44. Nayak, M. K., Mabood, F., Tlili, I., Dogonchi, A. S. & Khan, W. A. Entropy optimization analysis on nonlinear thermal radiative electromagnetic Darcy–Forchheimer flow of SWCNT/MWCNT nanomaterials. *Appl. Nanosci.* **11**(2), 399–418 (2021).
45. Vafai, K. Convective flow and heat transfer in variable porosity media. *J. Fluid Mech.* **147**, 233–259 (1984).
46. Vafai, K., Alkire, R. L. & Tien, C. L. An experimental investigation of heat transfer in variable porosity media. *J. Heat Transf.* **107**, 642–947 (1985).
47. Rees, D. A. S. & Pop, I. Vertical free convection in a porous medium with variable permeability effects. *Int. J. Heat Mass Transf.* **43**, 2565–2571 (2000).

48. Hayat, T., Haider, F., Alsaedi, A. & Ahmad, B. Unsteady flow of nanofluid through porous medium with variable characteristics. *Int. Commun. Heat Mass Transf.* **119**, 104904 (2020).
49. Ullah, I. Activation energy with exothermic/endergonic reaction and Coriolis force effects on magnetized nanomaterials flow through Darcy–Forchheimer porous space with variable features. *Waves Random Complex Media* **1**, 1–14. <https://doi.org/10.1080/17455030.2021.2023779> (2022).
50. Azhar, E., Maraj, E. N. & Iqbal, Z. Mechanistic investigation for the axisymmetric transport of nanocomposite molybdenum disulfide-silicon dioxide in ethylene glycol and sphericity assessment of nanoscale particles. *Eur. Phys. J. Plus* **133**(3), 1–12 (2018).
51. Anantha Kumar, K., Sandeep, N., Sugunamma, V. & Animasaun, I. L. Effect of irregular heat source/sink on the radiative thin film flow of MHD hybrid ferrofluid. *J. Therm. Anal. Calorim.* **139**(3), 2145–2153 (2020).
52. Nayak, M. K., Prakash, J., Tripathi, D. & Pandey, V. S. 3D radiative convective flow of ZnO-*SAE50* nano-lubricant in presence of varying magnetic field and heterogeneous reactions. *Propuls. Power Res.* **8**(4), 339–350 (2019).
53. Yin, C., Zheng, L., Zhang, C. & Zhang, X. Flow and heat transfer of nanofluids over a rotating disk with uniform stretching rate in the radial direction. *Propuls. Power Res.* **6**(1), 25–30 (2017).
54. Turkyilmazoglu, M. Nanofluid flow and heat transfer due to a rotating disk. *Comput. Fluids* **94**, 139–146 (2014).
55. Ali, B., Shafiq, A., Siddique, I., Al-Mdallal, Q. & Jarad, F. Significance of suction/injection, gravity modulation, thermal radiation, and magnetohydrodynamic on dynamics of micropolar fluid subject to an inclined sheet via finite element approach. *Case Stud. Therm. Eng.* **28**, 101537 (2021).
56. Aziz, A., Aziz, A., Ullah, I., Shah, S. I. & Alam, M. M. Numerical simulation of 3D swirling flow of Maxwell nanomaterial with a binary chemical mechanism and nonlinear thermal radiation effects. *Waves Random Complex Media* <https://doi.org/10.1080/17455030.2022.2066216> (2022).
57. Chu, Y.-M., Nazir, U., Sohail, M., Selim, M. M. & Lee, J.-R. Enhancement in thermal energy and solute particles using hybrid nanoparticles by engaging activation energy and chemical reaction over a parabolic surface via finite element approach. *Fractal Fract.* **5**(3), 119. <https://doi.org/10.3390/fractalfract5030119> (2021).
58. Li, Y.-M., Ullah, I., Alam, M. M., Khan, H. & Aziz, A. Lorentz force and Darcy–Forchheimer effects on the convective flow of non-Newtonian fluid with chemical aspects. *Waves Random Complex Media* <https://doi.org/10.1080/17455030.2022.2063984> (2022).
59. Khan, H. *et al.* The solution of twelfth order boundary value problems by the improved residual power series method: New approach. *Int. J. Model. Simul.* <https://doi.org/10.1080/102286203.2022.2051160> (2022).
60. Chu, Y. M., Bashir, S., Ramzan, M. & Malik, M. Y. Model-based comparative study of magnetohydrodynamics unsteady hybrid nanofluid flow between two infinite parallel plates with particle shape effects. *Math. Methods Appl. Sci.* <https://doi.org/10.1002/mma.8234> (2022).
61. Chu, Y. M., Nazir, U., Sohail, M., Selim, M. M. & Lee, J. R. Enhancement in thermal energy and solute particles using hybrid nanoparticles by engaging activation energy and chemical reaction over a parabolic surface via finite element approach. *Fractal Fract.* **5**(3), 119 (2021).
62. Uddin, I. *et al.* Thin film flow of carreau nanofluid over a stretching surface with magnetic field: Numerical treatment with intelligent computing paradigm. *Int. J. Mod. Phys. B* **36**(03), 2250021 (2022).
63. Abd El Salam, M. A., Ramadan, M. A., Nassar, M. A., Agarwal, P. & Chu, Y. M. Matrix computational collocation approach based on rational Chebyshev functions for nonlinear differential equations. *Adv. Differ. Equ.* **1**(2021), 1–17 (2021).
64. Jin, F., Qian, Z.-S., Chu, Y.-M. & ur-Rahman, M. On nonlinear evolution model for drinking behavior under Caputo-Fabrizio derivative. *J. Appl. Anal. Comput.* **12**(2), 790–806. <https://doi.org/10.11948/20210357> (2022).
65. Wang, F.-Z., *et al.* Numerical solution of traveling waves in chemical kinetics: Time-fractional fishers equations. *Fractals* **30**(2), 2240051. <https://doi.org/10.1142/S0218348X22400515> (2022).
66. Chu, Y. M., Khan, U., Zaib, A. & Shah, S. H. A. M. Numerical and computer simulations of cross-flow in the streamwise direction through a moving surface comprising the significant impacts of viscous dissipation and magnetic fields: Stability analysis and dual solutions. *Math. Probl. Eng.* **1**, 1. <https://doi.org/10.1155/2020/8542396> (2020).

Author contributions

Dr. I.U. contributed to the write up of the paper and drafted the final manuscript to the journal, Dr. Y.A. conceptualized and remodeled the problem Dr. A.A.P. solved the model problem through mathematical software as the corresponding revision part. Dr. M.A. revised the results and discussion part with physical amplifications and revision and proofreading of the whole manuscript. Dr. W.W. corrected the plotted and tabulated data and provided the validation of the result with published work.

Competing interests

The authors declare no competing interests.

Additional information

Correspondence and requests for materials should be addressed to W.W.

Reprints and permissions information is available at www.nature.com/reprints.

Publisher's note Springer Nature remains neutral with regard to jurisdictional claims in published maps and institutional affiliations.



Open Access This article is licensed under a Creative Commons Attribution 4.0 International License, which permits use, sharing, adaptation, distribution and reproduction in any medium or format, as long as you give appropriate credit to the original author(s) and the source, provide a link to the Creative Commons licence, and indicate if changes were made. The images or other third party material in this article are included in the article's Creative Commons licence, unless indicated otherwise in a credit line to the material. If material is not included in the article's Creative Commons licence and your intended use is not permitted by statutory regulation or exceeds the permitted use, you will need to obtain permission directly from the copyright holder. To view a copy of this licence, visit <http://creativecommons.org/licenses/by/4.0/>.

© The Author(s) 2022